

Electric organ discharge diversity in the genus *Gymnotus*: functional groups and electrogenic mechanisms

A. Rodríguez-Cattáneo¹, P Aguilera¹, E. Cilleruelo¹, W.G.R. Crampton², and A. A. Caputi¹

1. Departamento de Neurociencias Integrativas y Computacionales, Instituto de Investigaciones Biológicas Clemente Estable. Av. Italia 3318. Montevideo, Uruguay.
2. Department of Biology, University of Central Florida, 4000 Central Florida Blvd., Orlando, Florida, 32816, United States of America.

Corresponding Author: Angel Caputi email: angel@iibce.edu.uy

Key words: Fixed motor pattern, evolution, signal diversity, electrocytes, coordination, excitability

Summary

Previous studies describe six factors accounting for interspecific diversity of electric organ discharge (EOD) waveforms in *Gymnotus*. At the cellular level, three factors determine the locally generated waveforms: (1) electrocyte geometry and channel repertoire; (2) the localization of synaptic contacts on electrocytes surfaces; (3) electric activity of electromotor axons preceding the discharge of electrocytes. At the organismic level, three factors determine the integration of the EOD as a behavioral unit: (4) the distribution of different types of electrocytes and specialized passive tissue forming the electric organ (EO); (5) the neural mechanisms of electrocyte discharge coordination, (6) post-effector mechanisms. Here, we reconfirm the importance of the first five of these factors based on comparative studies of a wider diversity of *Gymnotus* than previously investigated.

Additionally, we report a hitherto unseen aspect of EOD diversity in *Gymnotus*. The central region of the EO (which has the largest weight on the conspecific-received field) usually exhibits a negative-positive-negative pattern where the delay between the early negative and positive peaks (determined by neural coordination mechanisms) matches the delay between the positive and late negative peaks (determined by electrocyte responsiveness). Because delays between peaks typically determine the peak power frequency, this matching implies a co-evolution of neural and myogenic coordination mechanisms in determining the spectral specificity of the intraspecific communication channel.

Finally, we define four functional species-groups based on EO/EOD structure. The first three exhibit a heterogeneous EO in which double-innervated electrocytes are responsible for a main triphasic complex. Group I species exhibit a characteristic cephalic extension of the EO. Group II species exhibit an early positive component of putative neural origin, and strong EO auto-excitability. Group III species exhibit an early, slow, negative wave of abdominal origin, and variation in EO auto-excitability. Representatives of Group IV generate a unique waveform comprising a main positive peak followed by a small, load-dependent negative component.

Introduction

The genus *Gymnotus* includes 37 species, distributed from Uruguay to as far north as southern Mexico (Crampton, 2011). These fishes, like other members of the order Gymnotiformes, exhibit the unusual ability to generate electric fields from a specialized electric organ (EO) controlled by the nervous system (Lissmann, 1958. Caputi et al., 2005, Caputi, 2011). The field generated by the electric organ discharge (EOD field) is affected by the presence of nearby objects. Changes to the ongoing transcutaneous fields (electric images) are evaluated by an electrosensory array, allowing the fish to analyze the structure of nearby objects (Pereira and Caputi, 2010).

In *Gymnotus*, the EOD field comprises a continuous train of pulses. Each pulse in the series is characterized by a stereotyped, species-specific waveform which serves as a communication signal, including for mate attraction, in addition to its role as an electrolocation carrier (Black-Cleworth, 1970; Westby, 1974; McGregor and Westby, 1992; Crampton and Albert 2006., Crampton et al. 2008, 2011).

It has been proposed (Bennett, 1971; Macadar, 1993; Caputi 1994, 1999; Caputi et al, 2005, Rodríguez-Cattáneo, 2009) that the structure and specificity of the EOD field waveform in pulse fish depends on variation in six different factors. Three of these, occurring at the cellular level of organization, determine the locally generated waveforms: (a) the geometry and channel repertoire of myogenic electrocytes; (b) the localization of the synaptic contacts on electrocytes surface; (c) the synchronous activity of a large bundle of electromotor axons preceding the discharge of electrocytes. The other three factors determine, at an organismal level, the integration of the EOD as a behavioral unit: (d) the distribution of different electrocyte types and specialized passive tissue forming the electric organ (EO); (e) the neural mechanisms of coordination of electrocyte activity; (f) the geometry and conductance of surrounding tissues. This last factor determines the post effector mechanisms of current summation along the fish's body and is essential to understand how the electromotive force pattern is transformed into an electric field in water (Aguilera et al., 2001; Caputi and Budelli, 2006).

The influence of these six kinds of variation on EOD waveform has been well documented by a long series of studies involving cellular and integrative analysis of the EOD in the model species *Gymnotus omarorum* (Trujillo-Cenóz et al., 1984; Lorenzo et al., 1988, 1990, 1993; Trujillo-Cenóz and Echagüe, 1989.; Macadar et al., 1989; Caputi and Trujillo-Cenóz, 1994; Caputi and Budelli, 1995; Sierra et al., 1995; 2005; Caputi et al., 1989, 1993, Caputi and Aguilera, 1996; Castelló et al., 2000; Aguilera et al., 2001; Rodríguez-Cattáneo and Caputi, 2009).

Comparative studies of other species have allowed us to describe an additional type of EO organization which influence the EOD field and its waveform. In *Gymnotus coropinae* (Rodríguez-Cattáneo et al., 2008; Castelló et al., 2009) we observed a unique pattern comprising a rostral extension of the hypaxial EO below the cleithrum aponeuroses. In this region of the EO, the electrocytes are large, few in number, and may be distinguished by their characteristic shape and innervation patterns (Castelló et al., 2009).

In another study of an as yet undescribed species (*G. n. sp.* "itu") , we showed that the electric organ auto-excitability suffices to explain the difference in waveform between two species whose EO and EOD are similar, except for late wave components resulting from the propagation of the action potential through the electrocyte membrane (Rodríguez-Cattáneo and Caputi, 2009).

Finally, in specimens of *G. carapo* from Suriname (*G. carapo* SU), we observed that the early positive component (which occurs only one and a half ms after the pacemaker discharge at about 200 mm caudal to the pacemaker location) is too early to be generated by miogenic mechanisms. This component is instead more likely the result of synchronized activity of the posterior electromotor nerve (Rodríguez-Cattáneo et al., 2008).

In this paper we test the hypothesis that signal diversity in *Gymnotus* may be explained by variation in the anatomo-functional features described above, and evaluate the role of the first five of the six factors previously recognized as determinants of interspecific waveform variation. Combining data from the seven species reported here with the four species studied earlier, we have now compiled electrophysiological and anatomical surveys for 11 species – including representatives of two (G1 clade and *G. carapo* clade) of the three major lineages of *Gymnotus* (G1 clade, G2 clade, and *G. carapo* clade sensu Lovejoy et al., 2010). Besides obtaining data which confirm the first five factors listed above as important determinants of EOD diversity, our observations also indicate, for the first time, that the sharpness of the power spectra and the peak power frequency is determined by the co-evolution of neural coordination mechanisms and electrocyte responsiveness.

Methods

Animals. Specimens of *G. sp.* "carapo PE", *G. curupira*, and *G. javari* were collected from rainforest creeks in the vicinity of the Instituto de Investigaciones de la Amazonia Peruana at Jenaro Herrera, Loreto, Peru (04°54' S, 073°39' W) by W.G.C. Authorization for field collections was provided by Ministerio de La Producción, Resolución Directorial No. 546-2009-PRODUCE/DGEPP (22 July 2009, Lima, Perú). Specimens of *G. obscurus*, *G. tigre*, and *G. varzea*, were collected from floodplain habitats of the Rio Amazonas within 50 km of the city of Iquitos,

Loreto, Peru (03°45' S, 73°15'W) by a local fish dealer. Specimens of *G. sylvius* were obtained from the Rio Paraná by local dealers in Esquina (Argentina).

All specimens were identified unambiguously to species by W.G.C. on the basis of external morphology, and by comparison to the primary types. Peruvian specimens reported here as *G. sp* “carapo PE” closely resembled those studied previously from Suriname (the region of the type locality for *G. carapo* - Albert and Crampton 2003) in both morphology and head-to-tail EOD (see Rodriguez-Cattáneo et al., 2008), but this species complex is the subject of ongoing taxonomic revision. For clarity we refer to *G. carapo* from Suriname as *G. carapo* SU.

We studied a total of 158 specimens: six *G. sp*. “carapo PE”(total length, TL, 70-247 mm), nine *G. curupira* (TL 120-219 mm), 119 *G. javari* (TL 85-240 mm), one *G. obscurus* (TL 170 mm), 20 *G. sylvius* (TL 196-420 mm), two *G. tigre* (TL 230-260 mm) and one *G. varzea* (TL 180 mm).

All experiments were either non-invasive or terminal. Protocols were approved by the Instituto de Investigaciones Biológicas Clemente Estable (Comisión de Bioética 001/03/2011) and University of Central Florida Institutional Animal Care and Use Committee (IACUC) (Protocol number 06-33W). They also followed the guidelines of the Comisión Honoraria de Experimentación Animal (Universidad de la República, Uruguay), the Society for Neuroscience, and the International Guiding Principles for Biomedical Research Involving Animals. Following recordings, fish were sacrificed by an overdose of pentobarbital (2 mg, repeated if necessary up to apnea and EOD cessation) and fixed for taxonomic or anatomical analyses as described below.

Evaluation of Head to tail EODs Far fields generated by the EODs were recorded in water at standardized temperature (27°C +/-0.1°C) and conductivity (55 +/- 1 μScm^{-1}). Each fish was allowed five minutes to acclimate to the aquarium. The recording arena was 80 cm long by 40 cm wide, and filled to 36 cm depth. Individual fish were placed within a nylon-mesh sock supported by a mesh cradle suspended in mid-water (17 cm depth) and positioned equidistant from the tank ends and walls. Signals were captured using nickel chromium electrodes placed at the tank ends. The electrodes were connected to a wide-band (0.1 Hz to 30 kHz) AC-coupled differential amplifier (Signal Recovery 5113). EODs were digitized using a National Instruments NI-USB 6216 digitizer at a sampling rate of 200 kHz and a resolution of 16 bits. Measurements of peak power frequency and signal duration were made using custom-written MATLAB and Java software designed by W.G.R Crampton. EOD durations were calculated with the beginning and end of the EOD taken at a 1% threshold of the amplitude of the normalized dominant positive phase. Spectral power densities were calculated from 65,536-point Fast Fourier Transform. EOD amplitude was measured as mV cm^{-1} at 10 cm at a standardized conductivity of 55 μScm^{-1} following the procedure described

by Franchina and Stoddard (1998). Specimens retained for taxonomic analysis alone were fixed with 10% formalin for 3-14 days, preserved in 70% ethyl alcohol, and deposited as voucher specimens at the Museo de Historia Natural de la Universidad Nacional Mayor de San Marcos, Lima, Peru, and at the University of Florida, Gainesville, USA.

Detailed spatial analysis of the EOD

For four *G. sp.* "carapo PE", six *G. curupira*, eight *G. javari*, one *G. obscurus*, 20 *G. sylvius*, two *G. tigre*, and one *G. varzea*, the *single air gap* procedure was utilized to characterize the net head to tail electromotive force of the EOD, and the *multiple air gap* procedure was utilized to characterize the detailed spatio-temporal patterns of the equivalent electromotive force.

The *single air gap* procedure consists of the simultaneous recording of the current and voltage drop across resistors connected between the head and the tail of the fish when it is suspended in air (Caputi et al., 1989). By changing the value of such resistance (R_o) we constructed a separate characteristic curve for the peak of each of the phases of alternating polarity in the EOD (its characteristic curve, Caputi et al., 1989, Rodríguez-Cattáneo and Caputi, 2009).

The ordinate intersection represents the peak EMF (which is different for each wave) and the absolute value of the slope represents the internal resistance (R_i , in general very similar across waves, Cox and Coates, 1938). In some species, wave components resulting from the activation of the electrocytes by the immediately preceding wave components show a parabolic relationship between current and voltage. This indicates a low excitability of the electrogenic membranes subservient to such components (Rodríguez-Cattáneo and Caputi, 2009).

The *multiple air gap* procedure allowed us to compare EOD waveforms generated by different regions of the fish's body (Caputi et al., 1993). Fish were suspended in air using a custom-made apparatus that holds the fish on a grill-like array of parallel wires. The wires in contact with the skin were perpendicular to the main axis of the body, one at each end of the fish and the other at the limits of each of the explored regions. Voltages were simultaneously recorded between pairs of wires, amplified to reach adequate amplitude for similar quantization (bit resolution always larger than 8 bits), sampled at 25 kHz, and analyzed using custom MATLAB software (written by E.C. and A.R.C.). For the purposes of this investigation, seven regions of the fish's body were considered; their lengths adapted to cover the whole length of the fish. Because of the different origins of the wave components, several recordings were obtained for each fish with different configurations before finding the montage yielding the most representative picture of the EOD pattern. In general, regions showing larger changes in EMF for any of the components were explored with a greater resolution. The length of the six caudal regions varied in integer multiples of 1 cm. The remaining rostral portion corresponded to the rest of the fish.

In the multiple air gap condition, load is absent. Therefore, voltage recordings are considered good estimators of the equivalent electromotive forces generated by different portions of the fish's body for the components that are directly activated by synaptic action. To compare the expression of EO activation mechanisms from diverse regions (with different spacing between electrodes, i.e. gap length), we measured the amplitude of each peak and then normalized this amplitude by the length of the gap, expressed as a percentage of total length.

Additional electrophysiological techniques. The electromotive force pattern of two species (*G. javari* and *G. obscurus*) showed specific features that could not be assessed completely by the multiple air gap technique. These features were: a) at the head and abdominal region of *G. javari* we found a complex EOD suggesting the presence of an expansion of the EO behind the cleithrum-opercular aponeuroses, as previously described in *G. coropinae* (Castelló et al., 2009); b) in *G. obscurus*, we noted what we will henceforth describe as a "facultative monophasic EOD", with a dominant positive component followed by a much lower-amplitude negative component, the amplitude of which is strongly dependent on the external load (Bell et al., 1976; Caputi et al., 1998; Rodríguez-Cattáneo and Caputi, 2009). To accommodate these novel features, three specimens of *G. javari* were explored with smaller size gaps (1 cm, starting from the snout) and one specimen using near-field recordings with the fish in water (see *near field analysis* below). In *G. obscurus* a differential load procedure was applied (see *simple air gap method with differential load* below).

a) Near field analysis was performed to confirm the presence of electrogenic sources at the head region as well as body sources of opposite polarity that are activated synchronously. Electric fields produced by the EOD were recorded with the fish resting in the middle of a net pen spanning between two ends of a plastic tank (45×26 cm filled with water up to 4 cm depth, with conductivity 30 μScm^{-1} , temperature 24°C). The back and forth movements of fish were minimized using stitches to adjust the net to body length. We recorded two variables: (i) the longitudinal EOD field using two silver electrodes, each one of them placed at the center of each narrow face of the tank, parallel to the mid-line of the fish (i.e. one in front of the head and the other behind the tail); (ii) the potential gradient perpendicular to the side of the body (near field) was measured along a line parallel to the fish skin at 2 mm distance from the closest point. Exploring electrodes tips (2.5 mm apart, perpendicularly aligned to the body axis) were moved from head to tail at a slow and constant speed using a motorized driver, the position of which was continuously monitored. The voltage drop between exploring electrodes was measured using a high-input impedance, high-gain differential amplifier (10 Hz to 20 kHz band-pass filter, in house constructed), and was digitized using a National Instruments 6016B digitizer at a sampling rate of 50 kHz and a resolution of 16 bits. For the analysis, we constructed a matrix where columns represent epochs of 10 ms before and

10 ms after the peak of the head to tail EOD taken at every mm ($\pm 200 \mu\text{m}$) along the recording line. These measurements allowed us to qualitatively estimate (because distance was not perfectly constant due to the curvature of the body and the position error) the current density flowing outward and inward to the fish at different times and at different sites along the body.

b) Simple air gap method with differential load. The tail region of the biphasic *G. obscurus* specimen was further explored using a variation of the simple air gap method (Bell et al., 1976, Rodríguez-Cattáneo and Caputi, 2009). We split the load into two, parallel “one-way”, paths of opposite direction using germanium diodes. By differentially changing the load on each branch we were able to explore the efficacy of the longitudinal currents generating V_3 for eliciting V_4 at the tail region. While one diode allows the current generating V_3 (I_3) to flow through an externally controlled resistive path and block the current generating V_4 (I_4), the other allows the circulation of I_4 through another externally controlled path, blocking I_3 . It is important to note that when the absolute values of peak voltages are lower than the cut-off threshold of the diodes (300 mV), current does not circulate in any direction. However, when the absolute values of peak voltages are larger than the diode threshold, they are controlled by the external load. We used an 11-position step switch to modify an external load connected in series with a diode oriented in such a way that allowed only the flow of I_3 . Thus, for a given position of the step switch we clamped the peak value of I_3 . For each of the 11 positions of the switch (i.e. for each value of I_3) we explored the voltage-current relationship of V_4 by varying the resistance of a rheostat connected in series with the second diode. At the end of this series of experiments, we obtained 11 characteristic curves, one for each position of the switch. Because we found that voltage current was well fitted by a linear decreasing function (see Results) we were able to estimate the electromotive force (EMF) generating V_4 (EMF₄) for each clamped value of I_3 .

Anatomy and innervation of the electrogenic tissue. One or two specimens of each species were fixed after euthanasia. The structure of the EO and the distribution of the thin nerve bundles, as well as the arrangement of the electromotor nerve terminals on the electrocytes’ surface were studied using silver impregnated samples. For this purpose, after a combined fixation and decalcification step (using De Castro’s formula, (Ramón y Cajal and De Castro, 1933)), a portion of the middle part of the body, and a portion of the tail, were silver impregnated (AgNO_3 , 1.5%, 7 days at 37°C) and subsequently reduced in formaldehyde-hydroquinone. Tissues were embedded in a soft mixture of epoxy resin and sectioned ($30 \mu\text{m}$ thick) either frontally or parasagittally. In two *G. javari*, the whole head and abdominal wall was fixed in formalin as a single piece. After decalcification, the cranium was removed. The remaining mandibular and abdominal wall regions were sectioned horizontally (200 micrometers) to search for a possible portion of the EO extending

into the head region as suggested by the electrophysiology. Sections were stained with a solution of methylene blue (1%), dehydrated, and mounted in resin. All slides were explored under a light microscope and digitally converted using a variety of optical and digital camera resolutions.

Nomenclature of waveform components

For the detailed spatial analysis of the EOD we use the wave components nomenclature introduced by Trujillo-Cenóz et al. (1984) for *G. omarorum* (Richer-de-Forge et al., 2009) with amendments by Rodríguez-Cattáneo et al. (2008). In figure 1 we describe the correspondence between this nomenclature and that introduced by Crampton and Albert (2006) for the far-field head-to-tail recordings. Is important to note that the nomenclature of the wave components is not only based on the electrophysiological recordings, we also take into account the presence of anatomical data suggesting by spatial correlation a generation mechanism. For each trace we first the main positive component, and find the presence of caudal innervated electrocytes in such region. Second, in traces where a negative peak preceded V₃ we identified the presence of rostrally innervated electrocytes to define this peak as V₂. Taking into account the curarization experiment (reported elsewhere, Caputi et al 1989; Caputi et al 1994; Caputi and Aguilera, 1996; Rodríguez-Cattáneo and Caputi, 2009) in which the activity following V₃ was shown as the consequence of electrocyte responsiveness we defined them as V₄ (first negativity after V₃) and V₅ (first positivity after V₃). In the case of V₁, we found two slow waves, one originated at the head (V_{1r}) and another one, positive, originated at the limit between the central and caudal region of the body. Finally, we found a particular V₃ associated with the presence of a rostral extension of the EO, this was studied in detail elsewhere and is referred to as V_{3r} (Castelló et al, 2009).

Results

The far-field head-to-tail EOD recorded in water

All species of *Gymnotus* exhibit a main positive wave peak (V₃) followed by a negative peak of species-dependent amplitude and duration (V₄, Fig. 1). *Gymnotus obscurus* differs from all other congeners in exhibiting a quasi-monophasic EOD in which the V₃ peak is followed by a very low amplitude, load-dependent V₄ peak. In all the remaining species, the EOD starts with slow negative components of low amplitude (V_{1rostral}, abbreviated to V_{1r}), and the V₃ peak is preceded by a negative peak (V₂). A low-amplitude, late positive component (V₅) is present in *G. sp.* “carapo PE”, *G. javari*, *G. sylvius*, and *G. tigre* and facultative in *G. curupira* (6 out of 9 specimens). An early positive component (V_{1ct} was observed in *G. sp.* “carapo PE”, *G. sylvius* and *G. varzea*). Finally, likely associated with sexual differentiation (Crampton et al. 2011), we observed differences in the amplitude of V₄ in *G. javari* and *G. curupira*. Metrics on the amplitudes of each

peak as well as the peak power frequency (PPF) of the head to tail recorded EOD are presented in Table 1.

The spatiotemporal pattern of electromotive force and its anatomical correlates

In the following sections we describe in detail the spatial analysis of the EOD waveforms and their morphological correlates for the seven newly studied species reported here.

***Gymnotus* sp. “carapo PE”.** The head to tail EOD waveform of this species recorded in air is hexaphasic, with the waveforms closely resembling those of *G. carapo* SU (see Rodríguez-Cattaneo et al. 2008).

Before the principal peak (V_3) occurs (Fig 2A), there are a series of deflections comprising a brief low amplitude positive phase (V_{1ct}) flanked by two negative phases, V_{1r} and V_2 (see Fig. 2B at another scale for the detailed pattern). After the main positive peak there is a sharp negative wave (V_4) followed by a smooth positive wave (V_5). With the multiple air gap method (Fig 2C), these components can be identified as independent because, although they partially overlap in time, their spatial domains are clearly confined to discrete regions at different positions along the body coinciding with a plausible anatomical substrate for explaining their generation.

As in most species of *Gymnotus*, V_1 is generated in the abdominal region and V_2 in the central part of the body (Fig 2C-F). Accordingly, at abdominal and central regions of the EO, Cajal’s silver impregnations (Fig 2G) show very large double innervated electrocytes. The early positive component (V_{1ct} , Fig 2C arrow) is generated at about the transition between the central and tail regions of the fish’s body. The very early appearance of this component, and the presence of a large posterior electromotor nerve at the generation site suggest a possible neural origin. The three last wave components (V_3 , V_4 and V_5) are generated all along the EO receiving the contribution of caudally-innervated electrocytes mainly at the tail where they are more densely packed (Fig. 2 D-H). Peak amplitude measured in volts per unit length of the recorded portion increases as the electrocyte density in a rostral-caudal direction along the domain of every component except for V_{1r} and V_{1ct} , which are instead very localized (Fig. 2 D-H).

***Gymnotus curupira*.** This species is tetraphasic. The electromotive force pattern generated by this species is similar to that shown by *G. omarorum* although the amplitude of the EOD in *G. curupira* is weaker than in *G. omarorum* (Caputi et al., 1993; Rodríguez-Cattáneo and Caputi, 2009) for every component, and the regional waveforms have a higher peak power in every region of the body (Fig 3). Anatomical studies suggest that V_1 is generated at the abdominal region by the rostral faces of doubly innervated electrocytes; V_2 (Fig 3A-B) is generated at the central region by the rostral faces of very large double innervated electrocytes at the central region of the EO and the complex V_3 and V_4 along all the EO generated by all electrocytes (Fig 3C-E). Peak amplitude

measured in volts per unit length of the recorded portion increases in a rostro-caudal direction along the domain of every component (Fig 3C-D). In some specimens V_4 ends with a gradual decline in voltage, as does the V_4 component of *G. omarorum* but in other there is a clear V_5 .

***Gymnotus javari*.** The spatiotemporal pattern of electromotive force and the anatomy of *G. javari* are much closer to those documented in *G. coropinae* (Castelló et al., 2009, Rodríguez-Cattáneo et al, 2008) than to other species (4A).

Electrogeneration starts at the head, where a very slow head negative component (V_{1r}) is followed by a head positive peak (V_{3r} , Fig 4A-B). A multiple air gap with 1 cm resolution showed that these components are generated at the peri-opercular region (Fig. 4B).

Consistently, anatomy revealed electrocytes in the posterior region of the head. A ventral view of the superimposed traces, outlining the electrogenic structures observed in serial horizontal sections of the abdominal wall and floor of the mouth (Fig. 5A). As observed in the horizontal and oblique sections (Fig 5B), a row of electrocytes is aligned parallel to the aponeurotic sheath connecting the operculum to the cleithrum. At approximately the midline, another pair of longitudinal rows of electrocytes (continuing the abdominal regions of the EO) converges with these two oblique rows to form an arrow like profile (Fig 5A). The quality of our material was not sufficient to analyze the innervation pattern of this portion of the EO. However, comparative analysis with *G. coropinae* and near field recordings (see below) suggest that these portions are responsible for the slow and rostral V_{1r} - V_{3r} complex. The pattern observed at the central and caudal regions of the body (Fig 5C) can be explained as in other multiphasic species. A dorsal row of long, double-innervated electrocytes, present from the abdominal to the tail region may explain V_2 . However one must remark that in this species V_2 has two peaks at different distances from the snout (25% and 75% of fish length, respectively, Fig 4C). The caudal quarter of the body has four similar rows of small caudally innervated electrocytes with smaller inter-electrocyte distances (Fig 5D). Finally, the complex V_{3-4-5} extends from the abdominal region to the tip of the tail and increases in amplitude in a rostro-caudal direction (Fig. 5 C-D).

Our discovery of electrogenic tissue extending rostrally into the head region motivated us to illustrate a higher resolution electrophysiological analysis of the near field in detail (Fig. 6). Recordings of near fields adjacent to the fish's body taken perpendicular to the skin confirmed the hypothesis that the very early negative potential (V_{1r}) is generated at the rostral expansion of the EO (Fig. 6A and B). The field is very complex at the time labeled as t_2 in figure 6A and C. Rostrally, it shows two reversal points flanking a large sink, with the rostral source sharply localized, and the caudal source exhibiting two maxima. These findings suggest that the near field around the head is dominated by the local generators. This local field has important differences with the far field (Fig

5A, inset), which is instead dominated by the generators at the central and tail regions of the fish's body and yields the main components V_3 , V_4 , and V_5 (times t_3 - t_6 in Fig 5D-G).

***Gymnotus obscurus*.** The single specimen available for this species exhibited a biphasic head to tail EOD in the simple airgap comprising a dominant positive component (V_3) followed by a low amplitude negative component (V_4 , Fig. 7A inset). The negative component (V_4) was load-dependent, such that with decreasing external resistance exhibited a mild increase in amplitude (Fig 7A inset; compare black trace under low resistance load and red under high resistance load). This different behavior of V_3 and V_4 are described by the characteristic curves (Fig. 7A and B respectively). This motivated the detailed analysis of this feature under the differential load procedure introduced by Bell et al. (1976) and applied by Rodríguez-Cattáneo and Caputi (2009) for the analysis of a similar problem in the tail region of *G. omarorum*. Clamping the longitudinal current associated with V_3 (I_3), we were able to construct ten different characteristic curves of V_4 (for the sake of clarity only five graphs were superimposed in Fig 7C). The slopes of these plots are similar, and the ordinate values of the fitting lines increase with I_3 (Fig 7D). This confirms that V_4 is load dependent and indicates that the auto-excitability of the EO in this species is markedly lower than in other species of *Gymnotus*.

The multiple air gap procedure demonstrated that *G. obscurus* has two wave components: a large positive one, and a very small negative, load dependent component (V_4). The spatiotemporal pattern of electromotive force (Fig 7E) shows that V_3 is generated all along the EO and increases exponentially from head to tail while V_4 is generated at the caudal third of the fish's body. In this caudal third, the ratio V_4/V_3 also increases in a rostral-caudal direction.

A single sample of the central region of the EO of this specimen was analyzed anatomically. In this sample, we found four rows of flat electrocytes on each side. We were unable to find rostral innervation of the electrocytes of the dorsal row of the EO (Fig 7F).

***Gymnotus sylvius*.** Similarly to *G. carapo* SU, the head to tail EOD waveform of this species recorded in air, by the single air gap method, is hexaphasic. Before V_3 , there is a series of two smooth deflections (V_{1r} - V_{1ct}) and one sharp peak (V_2). After V_3 , a sharp negative (V_4) wave and a smooth positive (V_5) wave were observed in all specimens (Fig. 8A). However, compared to *G. carapo*, *G. sylvius* shows larger EMF and synchrony.

The multiple air gap method shows that the two small and early components observed in the head to tail (V_{1r} - V_{1ct}) can be identified as independent because of their different origin along the body (Fig 8B). As in *G. carapo* SU (Rodríguez-Cattáneo et al., 2008) the negative component (V_{1r}) starting the EOD waveform is generated abdominally and the positive component (V_{1ct}) is generated at about the transition between the central and tail regions of the fish's body.

At the central region of the EO consists of a dorsal row of very large double innervated electrocytes explaining V_2 (Fig 8 C and F) and three rows of small caudally innervated electrocytes on each side explaining the complex V_{345} . The caudal quarter has four similar rows of small caudally innervated electrocytes, which exhibit a smaller inter-electrocyte distance explaining the larger peak amplitude of the measured complex V_{345} . Consistently with the neurogenic hypothesis of V1ct a large electromotor nerve is observed at the transition between the central and tail regions (Fig D, E and G).

***Gymnotus tigre*.** The head to tail waveform of this species recorded in air is pentaphasic, showing a negative V_{1r} and a late positive V_5 besides the main complex V_{2-3-4} . The spatiotemporal pattern of electromotive force (Fig 9A) shows that V_1 is generated at the abdominal region, V_2 at the central region and the complex V_{3-4} along the entire EO. At gaps 4, 5 and 6, a small V_5 was observed in the two studied specimens. The electromotive force of all components increases in a rostro-caudal direction within their regional domains. As expected from this pattern, the central region of the EO consists of four rows of electrocytes with a dorsal row of double innervated electrocytes (Fig 9B). At the tail region there are four rows of small and caudally innervated electrocytes (Fig 9C).

***Gymnotus varzea*.** We procured a single specimen of *G. varzea* for this study. The head to tail waveform of this species recorded in air is tetraphasic. In the air gap analysis of this single specimen, only six gaps were obtained (the activity of the most caudal gap was not recorded because the tip of the tail moved during the experiment). The spatio-temporal pattern of electromotive force (Fig 10A) indicates that in this species V_1 is generated at the abdominal region, and the complex V_{2-3-4} is generated at the rest of the fish's body. In the last available gap, which in this specimen comprised the anterior portion of the tail, a biphasic pattern preceded by the activity of the posterior electromotor nerve was observed (Fig 10A arrow). Consistently with this pattern, at the abdominal and central regions, a dorsolateral row of electrocytes is innervated in both faces at the tail only single innervated electrocytes are observed.

Discussion

Waveform diversity can be explained by a combination of five different anatomico-functional factors.

We have studied 11 species belonging to two of the three main clades of the genus *Gymnotus* (Lovejoy et al., 2010). To facilitate the description and discussion of EOD diversity, we have grouped the known EOD patterns into four main Anatomico-functional groups based on the combination of mechanisms as it is described in table II.

Group I is represented by two species in our studies, *G. coropinae* and *G. javari*, both small species with a weak EOD that clearly exhibits two components in terms of frequency components and generation sites: (a) a sharp multiphasic component with a peak power at very high frequency ranges generated at the central and caudal regions; and (b) a slower component with a power spectra peaking at lower frequencies generated by an expanded region of the EO that protrudes into the head under the cleithral aponeurotic sheath. The abdominal region contributes to both components.

The slow component generated mainly at the head extension of the EO, can be described with the multiple air gap by two main deflections generated at the innervated faces of the electrocytes. The head negative deflection originates from rostrally innervated electrocytes and is represented in the near field by a source at the bi-opercular level. The head positive deflection is a peak preceding the caudally generated multiphasic component. This peak (which is broader and earlier than that generated at the central and caudal regions) is caused by the activation of the lateral faces of very large electrocytes. These electrocytes, which are oriented along the cleithrum, create sinks at both of the opercula, and a single source at the oral and perioral region.

The sharp multiphasic component consists of a $V_{2-3-4-5}$ sequence in which the origin of the different waves reflects the different innervation pattern of the EO. The sequence originating at the central region has its anatomical counterpart in the presence of a row of double innervated electrocytes on the same longitudinal domain. Rostral innervation of these double-innervated electrocytes explains the head negative onset of this multiphasic discharge at the central region. Caudal innervations of the remaining electrocytes in this region explain the presence of the main positive component (V_3). Likewise, the large autoexcitability of the EO explains the sharpness of V_4 and the presence of V_5 . The contribution of the more caudal portion of the fish body, where only singly innervated electrocytes are present consists of a V_{3-4-5} sequence. Neither in *G. coropinae* nor in *G. javari* was V_4 load dependent, confirming that current flow along the EO in the absence of external load is enough to recruit synchronously the rostral phases of the electrocytes. This sharp and load independent V_4 , as well as the back activation of some caudal faces at a short delay (V_5) indicates the high autoexcitability of the electrocytes *in situ*.

Together, these data suggest that the cephalic expansion of the EO in *G. javari* is functionally equivalent to the cephalic expansion of the EO in *G. coropinae* (Castelló et al., 2009). This expansion may generate a short-range field component, which is particularly strong around the head where the electroreceptive fovea occurs (Castelló et al., 2000). Because of the short range and the high resolution of the target electrosensory mosaic, we have shown in *G. omarorum* (Aguilera et al 2001) and *G. coropinae* (Rodríguez-Cattáneo et al, 2008; Castelló et al, 2009) that this rostral

component of the EOD is likely to carry active electrolocation signals while the higher voltage electric field generated by the central and tail regions of the body is likely to carry longer-range electrocommunication signals. In fact, concordant with the generality of this hypothesis, analyses of wave duration indicate that *G. javari* shows is an extreme example. The relatively long duration of head and abdominal generated components of the field restricted to a small region surrounding the head, and thus serving foveal electro location contrast with the fast discharge of the rest of the fish body reaching longer distance and thus serving communication. All this suggest that in this anatomo-functional group electrolocation and electro-communication carrier are well separated in two different frequency bands.

Group II comprises species with tetraphasic or pentaphasic EODs generated from the abdominal region to the tip of the tail. This group includes *G. curupira*, *G. sp. "itu"*, *G. omarorum*, *G. tigre*, and *G. varzea*. The EOD waveform always starts with a smooth negative component generated at the abdominal region (V_{1r}) and is followed by a complex V_{2-3-4} with a characteristic peak to peak ratio and associated delays. In group II, interspecific variation in the head to tail recorded waveforms mainly depends on the extent to which the rostral face of the electrocytes is excitable (see above). The ability of action potentials to excite the rostral faces is not an all-or-nothing trait. Some species (*G. curupira* and *G. sp. "itu"*) having large auto-excitability show the largest and sharpest V_4 , and may also show a small late positive component (V_5). At the other extreme, *G. omarorum* shows low autoexcitability which generate a small V_4 . In between these extremes, the remaining species exhibit intermediate amounts of auto-excitability, with consequently intermediate V_4 parameters. We should stress that EO autoexcitability is a phenotypically plastic character that is expected to vary over the course of an individual fish's life because of temperature, acclimation, and sexual differentiation (Caputi et al, 1998). Nevertheless, the study of a large number of specimens of *G. sp. "itu"* and *G. omarorum* captured from the Rio de La Plata basin throughout the year (in both the austral winter and summer, and during breeding and non-breeding seasons) indicated that the graded expression of V_{4-5} may be the only consistent species specific difference in electrogeneration mechanisms. (Rodríguez-Cattáneo and Caputi, 2009).

Group III is characterized by the presence of an early positive slow wave of neural origin at the head to tail electric field (V_{1ct}) and a large auto-excitability of electrocytes – indicated by the sharpness and load independence of V_4 and the presence of V_5 . This group includes *G. sp. "carapo PE"*, *G. carapo* SU, and *G. sylvius*. V_{1ct} could be explained by the presence of a large posterior electromotor nerve whose synchronic activation occurs at the same time as V_{1r} . Three arguments favor this interpretation: (1) the coincident timing of V_{1ct} with the activation timing of the nerve

observed as a minor deflection in the caudal gaps recordings in all species; (2) the coincidence of the location of the electric source of V_{1ct} with the site where the nerve reaches its largest diameter; and (3) the resistance to curare in *G. sylvius* (Caputi, Aguilera and Rodríguez-Cattáneo, in preparation).

The sharpness of V_4 and the presence of V_5 is generally associated with greater EO autoexcitability, as previously described (Rodríguez-Cattáneo and Caputi, 2009). In fact, curarization abolishes V_4 and V_5 in all Group III species tested, including *G. sp.* “carapo-PE”, *G. carapo* SU, and *G. sylvius*, indicating that these components are the consequence of the auto-excitability of the EO. As expected for very excitable electrogenic tissue, V_4 does not depend on load in species belonging to group III.

Group IV currently comprises a single species, *G. obscurus* (first discovered in the Brazilian Amazon: Crampton et al. 2005), in which the EOD begins with the main positive wave (V_3) and in which a preceding V_2 phase is absent. In addition to exhibiting a quasi-monophasic EOD, the single specimen of *G. obscurus* available for study exhibited three distinctive features: (1) the late negative peak occurs at the tail region and its electromotive force is highly dependent of the amount of longitudinal current associated with V_3 . (2) In the EO sample taken from this species we did not see rostral innervations in any of the electrocytes observed. (3) According to Lovejoy et al (2010), this type of EOD is derived from an ancestral multiphasic EOD state, implying loss of synapses on the rostral electrocyte faces, and a reduction of electrocyte excitability. Of the 37 species of *Gymnotus* described to date, only two other species, *G. cylindricus* and *G. maculosus* were known to generate a positive peak (V_3) followed by a very low-amplitude negative component (Kirschbaum, 1995). Similarly to our results in *G. obscurus*, the anatomical study of a region of the EO in those specimens failed to show double innervated electrocytes (Kirschbaum, 1995). Nonetheless, confirming the absolute lack of double innervated electrocytes in the three species is required to affirm that *G. cylindricus* and *G. maculosus*, belong to the same functional group as *G. obscurus*.

Phylogenetic distributions of the four functional groups:

The two species that we assigned to functional group I, *G. coropinae* and *G. javari*, belong to the G1 clade of Lovejoy et al. (2010). Other members of this clade are also known to exhibit similar EODs with high peak power frequencies (typically >1.8 kHz). These species are predicted to also exhibit the same rostral extension of the EO, and auto-excitability at the caudal region. These characteristics are fundamentally different from other species of *Gymnotus* that we examined,

and match the phylogenetic position of G1 species, as sister taxon to all remaining *Gymnotus* species in a deep evolutionary divergence.

All members of functional group II belong to the *G. carapo* clade of Lovejoy et al. (2010) (Lovejoy pers. comm. for *G. omarorum* and *G. sp. "itu"*). Likewise, all members of functional group III also belongs to the *G. carapo* species clade (Lovejoy et al. 2010) (Lovejoy pers. com. for *G. sylvius* and *G. carapo* SU), within a complex of species that are very closely related to *G. carapo* SU. The single member of functional group IV, *G. obscurus*, also belongs to the *G. carapo* clade of Lovejoy et al. (2010).

These patterns indicate that all species in the G1 clade of Lovejoy et al. (2010) share a common functional EOD pattern, that of Group I. In contrast, there is considerable diversity of waveform generation within the *G. carapo* clade, corresponding to functional groups II, III, and IV. In most cases this diversity is the consequence of the presence or absence, or relative amplitude of low amplitude EOD components. *G. obscurus*, with its unusual group IV EOD pattern is well nested within the *G. carapo* clade, indicating that radical modifications of EOD generation can evolve as a derived condition within this group (Lovejoy et al. 2010). Lovejoy et al's. (2010) phylogeny also contains a third, "G2 clade" comprising *Gymnotus cataniapo*, *Gymnotus pedanopterus*, and *Gymnotus cf. anguillaris*. We as yet do not have complete data sets for the EOD generation in any species belonging to the G2 clade, and this represents an important direction for future research.

The central EOD and the co-evolution of neural and peripheral mechanisms of electrogenesis. The central regions of the body of *Gymnotus* exhibit a pattern generated by the successive neural activation of rostral and caudal faces (V_2 - V_3), and also by the subsequent activation of rostral faces by the action potentials arising in the caudal faces (V_4). The intermediate values of electromotive force and internal resistance of the central region of the fish's body determine that the waveform generated here contributes to the far field waveform much more than rostral and caudal portions of the body (Caputi and Budelli, 1995). The interval V_2 - V_3 is a neurally determined delay. We have so far confirmed this feature using partial curarization (Rodríguez-Cattáneo and Caputi, 2009). On the other hand, the interval V_3 - V_4 is only dependent on the electrocyte excitability, since V_4 is generated by action potentials firing at the non-innervated faces when the action currents causing V_3 depolarize them above the critical firing level. We have postulated the co-evolution of neural and peripheral mechanisms responsible for the timing of the main sequence V_{3-4-5} (Castelló et al., 2009). Here we confirmed this hypothesis by including an additional six multiphasic species. The delay V_3 - V_4 (i.e. a peripherally determined sequence)

follows an increasing function of the delay V_2 - V_3 (a neurally determined sequence, Fig 11). Interestingly, in this plot one can identify regions corresponding to the position of each group.

The matching of the timing of central and peripheral determined temporal organization of the EOD raises the question on how electroreceptors tuning matches the peak power frequency. Although extensive data is available on matching receptor tuning curves with local EODs (Bastian , 1976, 1977, Watson and Bastian 1979, Yager and Hopkins, 1993) matching across species is still lacking and should be studied.

In addition one might speculate on the mechanisms needed to implement such a match. Changes of the V_2 - V_3 interval requires change in the presynaptic timing of the electromotor fibers. This can be achieved by changes in channel repertoire, distance between Ranvier nodes and/or fiber thickness (determining conduction velocity) or fiber lengths. On the other hand changes in electrocyte responsiveness (V_3 - V_4) are likely depending on channel repertoire or electrocyte geometry. Reasoning with parsimony may favor the hypothesis that a species-specific structural change of a membrane channel (or a group of channels) might be on the basis of this mechanism.

This matching of the timing of neural and peripherally determined inter-component intervals is important for sharpening the peak power frequency of the “communication carrier” characteristic of each species (Rodríguez-Cattáneo et al., 2008). Since the central region is the most importantly expressed in the head to tail EOD waveform, as well as the EOD waveform “seen” by conspecifics, this suggests that the frequency range of the power spectra may be a major important EOD feature for conspecific recognition (Hopkins, 1976) or for predator avoidance (Stoddard, 1999). Nonetheless, Crampton et al. (2011) documents cases of ecologically co-occurring species of *Gymnotus* that exhibit overlapping peak power spectral properties among mature adults, suggesting that species recognition may involve additional cues, such as the temporal properties of the head to tail EOD waveform (or parts of the waveform).

In conclusion. Present evidence from 11 species supports the notion that EOD waveform diversification in *Gymnotus* involved a combination of different anatomo-functional factors, which we summarize below in two categories: first those which are cell-based, and second those which act at the organismal level. In this study we identified the role of these factors for determining waveform diversity and identified four functional groups (Table 2). The early divergence between species in the G1 clade and other *Gymnotus* lineages is supported by strong differences in the EO organization, in which the presence of a rostral expansion of the EO is characteristic of species belonging to the G1 clade (sensu Lovejoy et al., 2010). Finally, the neural coordination mechanisms determining the wave timing are important for determining interspecific variation in the peak power frequency of the far field signals, which would not be possible if the electrocyte responsiveness did

not match the difference in neural volley delays. The strong correlation between the neutrally (V_2 - V_3) and the myogenically (V_3 - V_4) determined intervals among all species studied to date suggests a hitherto unseen co-evolution of neural and myogenic mechanisms, and supports the presence of a peak frequency in the power spectral density of the emitted signals.

Acknowledgements

We thank to the following, whose collaboration made possible the Amazonian study: a) Dr. Hernan Ortega (Departamento de Ictiología, Museo de Historia Natural de la Universidad Nacional Mayor de San Marcos) for graciously hosting this research expedition and organizing field permits; b) Euridice Honorio and Edwin Correa Verdi (Instituto de Investigaciones de la Amazonia Peruana for use of the Jenaro Herrera Research Center); c) Dr. Jorge L. Marapara Del Águila and his collaborators (Universidad de la Amazonia Peruana, Iquitos, Perú) for graciously providing laboratory space and fundamental support for the electrophysiological recordings and extraction of the anatomical samples. d) Erika Vanessa Correa and Maria Isabel Aldea Guevara for coordinating and assisting with field research and logistics; e) Joseph Waddell, Jeffrey Lambert, and John Stark from the University of Central Florida (UCF), and Edinson Emiliano Irarica Curinuqui, Rider Souza Chota, Nolortegui Parana Canelao, Edinson Irarica Huanaquiri, Hugo Irarica Huanaquiri for field and laboratory assistance and f) Alejandra Pastorino for technical processing of histological samples. We thank N. Lovejoy for fruitful discussions.

Funding: This research was funded by a) NSF grant DEB-0614334 to W. Crampton (PI) and to J. Albert, N. Lovejoy, and A. Caputi (co-PIs); b) grant from the European Commission ICT-FET proactive initiative 'embodied intelligence' (Project acronym: ANGELS, Grant No. 231845) and c) the Agencia Nacional de Investigación e Innovación of Uruguay (FCE 655 and SNI).

Bibliography

- Aguilera P.A., Castelló M.E., Caputi A.A.** (2001). Electoreception in *Gymnotus carapo*: differences between self-generated and conspecific-generated signal carriers. *J. Exp. Biol.* **204**,185-98.
- Albert, J. S. and Crampton, W. G. R.** (2003). Seven new species of the Neotropical electric fish *Gymnotus* (Teleostei: Gymnotiformes) with a redescription of *G. carapo* (Linnaeus). *Zootaxa* 28: 1-54.
- Bastian, J.** (1976). Frequency response characteristics of electoreceptors in weakly electric fish (Gymnotidae) with a pulse discharge. *J. Comp. Physiol. A* **112**,165 -180.
- Bastian, J.** (1977). Variations in the frequency response of electoreceptors dependent on receptors location in weakly electric fish (Gymnotidae) with a pulse discharge. *J. Comp. Physiol. A* **121**,53 -64.
- Bell, C. C., Bradbury, J. and Russell, C. J.** (1976). The electric organ of a mormyrid as a current and voltage source. *J. Comp. Physiol. A* **110**, 65 -88.
- Bennett, M. V. L. and Grundfest, H.** (1959). Electrophysiology of electric organ in *Gymnotus carapo*. *J. Gen. Physiol.* **42**,1067 -1104.
- Bennett, M. V. L.** (1971). Electric organs. In *Fish Physiology*, vol. V (ed. W. S. Hoar and D. J. Randall), pp. 347-491. London: Academic Press.
- Black-Cleworth, P.** (1970). The role of electrical discharges in the non-reproductive social behaviour of *Gymnotus carapo* (Gymnotidae, Pisces). *Anim Behav* **3**:1-77
- Caputi, A. A.** (1994) Integración de la descarga del órganos eléctrico en Gymnótidos de pulso. PhD thesis. Facultad de Ciencias (PEDECIBA).
- Caputi, A. A.** (1999). The electric organ discharge of pulse *gymnotiforms*: the transformation of a simple impulse into a complex spatio-temporal electromotor pattern. *J. Exp. Biol.* **202**,1229 -1241.
- Caputi, A. A.,** (2011). Electric Organs in: *Encyclopedia of Fish Physiology*. (Anthony Farrell, ed.) Academic Press.
- Caputi, A., Macadar, O. and Trujillo-Cenóz, O.** (1989). Waveform generation in *Gymnotus carapo*. III. Analysis of the fish body as an electric source. *J. Comp. Physiol. A* **165**, 361–370.
- Caputi, A., Silva, A. and Macadar, O.** (1993). Electric organ activation in *Gymnotus carapo*: spinal and peripheral mechanisms. *J. Comp. Physiol. A* **173**, 227–232.
- Caputi, A. and Trujillo-Cenóz, O.** (1994). The spinal cord of *Gymnotus carapo*: the electromotorneurons and their projection pattern. *Brain Behav. Evol.* **44**, 166–174.

- 641 **Caputi A. A. and Budelli .** (1995) The electric image in weakly electric fish: I. A data
642 based model of waveform generation in *Gymnotus carapo*. *J. Comput Neurosci* **2**, 131:147
- 643 **Caputi, A. and Aguilera, P.** (1996). A field potential analysis of the electromotor system
644 in *Gymnotus carapo*. *J. Comp. Physiol. A* **179**, 827–835.
- 645 **Caputi, A., Silva, A. and Macadar, O.** (1998). The effect of environmental variables on
646 waveform generation in *Brachyhypopomus pinnicaudatus*. *Brain Behav. Evol.* **52**, 148 -158
- 647 **Caputi, A. A., Carlson, B. and Macadar, O.** (2005) Electric organs and their control. In
648 Electoreception (Bullock, TH; Hopkins, CD; Popper AN, Fay RR eds.). Springer Handbook of
649 auditory research. Electoreception. v.: 21 , 1st, p.: 410 - 451, New York.
- 650 **Caputi, A. A. and Budelli, R.** (2006). Peripheral electric imaging in freshwater electric
651 fish. *J. Comp. Physiol. A* **192**, 587 -600.
- 652 **Castelló, M. E., Aguilera, P. A., Trujillo-Cenóz, O. y Caputi, A. A.** (2000).
653 Electoreception in *Gymnotus carapo*: pre-receptor processing and the distribution of
654 electoreceptor types, *J. Exp. Biol.* **203**, 3279-3287.
- 655 **Castelló, M. E., Rodriguez-Cattaneo, A., Aguilera, P. A., Iribarne, L., Pereira, A. C.,**
656 **and Caputi, A. A.** (2009) Waveform generation in the weakly electric fish *Gymnotus coropinae*
657 (Hoedeman): the electric organ and the electric organ discharge. *J. Exp. Biol.* **212**, 1351-1364
- 658 **Cox, R.T., and Coates, C.W.** (1938) Electrical Characteristics of the Electric Tissue of the
659 Electric Eel, *Electrophorus electricus* (Linnaeus). *Zoologica*, **23**, 203
- 660 **Crampton, W.G.R.** (2011). An ecological perspective on diversity and distributions. Pp.
661 165-189. In: *Historical Biogeography of Neotropical Freshwater Fishes* (Eds. J.S. Albert & R.E.
662 Reis). University of California Press, Berkeley
- 663 **Crampton, W. G. R., and J. S. Albert.** (2006). Evolution of electric signal diversity in
664 gymnotiform fishes. I. phylogenetic systematics, ecology and biogeography. Pp. 647-696; 718-731.
665 in: *Communication in Fishes*. (F. Ladich, S. P. Collin, P. Moller, and B. G. Kapoor, eds.) Science
666 Publishers, Enfield, N.H.
- 667 **Crampton, W. G. R., Thorsen, D. H., and Albert, J. S.** (2005). Three new species from a
668 diverse, sympatric assemblage of the electric fish *Gymnotus* (Gymnotiformes, Gymnotidae) in the
669 lowland Amazon basin, with notes on ecology. *Copeia*, **2005**, 82-99.
- 670 **Crampton, W. G. R., Davis, J. K., Lovejoy, N. R., and Pensky, M.** (2008). Multivariate
671 classification of animal communication signals: A simulation-based comparison of alternative
672 signal processing procedures using electric fishes. *Journal of Physiology, Paris* **102**, 304-321.

- 673 **Crampton, W. G. R., Lovejoy, N. R., and Waddell, J.C.**, (2011) Reproductive character
674 displacement and signal ontogeny in a sympatric assemblage of electric fishes. *Evolution* 65, 1650-
675 1666.
- 676 **Franchina, C.R., Stoddard, P.K.** (1998) Plasticity of the electric organ discharge
677 waveform of the electric fish *Brachyhypopomus pinnicaudatus* : I. Quantification of day-night
678 changes. *Journal of Comparative Physiology A* 183:759-768
- 679 **Hopkins, C. D.** (1976). Stimulus filtering and electroreception: tuberous electroreceptors in
680 three species of gymnotoid fish. *J. Comp. Physiol. A* **111**, 171–207.
- 681 **Kirschbaum, F.** (1995). Discharge types of gymnotiform fishes. pp. 172-180, In Moller, P.
682 (1995). Electric fishes: history and behavior. In *Chapman & Hall Fish and Fisheries Series*; 17, pp.
683 xxiv, 584. London, New York: Chapman & Hall.
- 684 **Lissmann, H. W.** (1958). On the function and evolution of electric organ in fish. *J. Exp.*
685 *Biol.* **35**, 156-191.
- 686 **Lorenzo, D., Velluti, J. C. and Macadar, O.** (1988). Electrophysiological properties of
687 abdominal electrocytes in the weakly electric fish *Gymnotus carapo*. *J. Comp. Physiol.* **162**, 141–
688 144.
- 689 **Lorenzo, D., Sierra, F., Silva, A. and Macadar, O.** (1990). Spinal mechanisms of electric
690 organ discharge synchronization in *Gymnotus carapo*. *J. Comp. Physiol. A* **167**, 447–452.
- 691 **Lorenzo, D., Sierra, F., Silva, A. and Macadar, O.** (1993). Spatial distribution of the
692 medullary command signal within the electric organ of *Gymnotus carapo*. *J. Comp. Physiol. A* **173**,
693 233–238.
- 694 **Lovejoy, N. R., Lester, K., Crampton, W. G. R., Marques, F. P. L., and Albert, J. S.**
695 (2010). Phylogeny, biogeography, and electric signal evolution of Neotropical knifefishes of the
696 genus *Gymnotus* (Osteichthyes: Gymnotidae). *Molecular phylogenetics and evolution* **54**, 278-290.
- 697 **Macadar, O.** (1993). Motor control of waveform generation in *Gymnotus carapo*. *J. Comp.*
698 *Physiol A* **173**, 728–729.
- 699 **Macadar, O., Lorenzo, D. and Velluti, J. C.** (1989). Waveform generation of the electric
700 organ discharge in *Gymnotus carapo*. II. Electrophysiological properties of single electrocytes. *J.*
701 *Comp. Physiol. A* **165**, 353–360.
- 702 **McGregor, P.K., and Westby G.W.M.** (1992). Discrimination of individually
703 characteristic electric organ discharges by a weakly electric fish. *An. Behave.* 43, 977–986
- 704 **Pereira, A.C., and Caputi, A.A.** (2010) Imaging in electrosensory systems. *Interdiscip Sci.*
705 Dec;2(4):291-307. doi: 10.1007/s12539-010-0049-2.

- Ramón y Cajal, S. and De Castro, F.** (1933) Elementos de técnica micrográfica del sistema nervioso. Barcelona, Madrid, Buenos Aires: Salvat Editores.
- Richer de Forges, M., Crampton, W. G. R. and Albert, J. S.** (2009). A new species of *Gymnotus* (Gymnotiformes, Gymnotidae) from Uruguay: description of a model species in neurophysiological research. *Copeia*, **2009**, 538 -544.
- Rodríguez-Cattáneo, A.** (2009) Descripción del patrón de la descarga del Organo Eléctrico en seis especies de *Gymnotus*. Facultad de Ciencias, Uruguay. Master Thesis (UDELAR-PEDECIBA).
- Rodríguez-Cattáneo, A., Pereira A. C., Aguilera P. A., Crampton W. G. R., and Caputi, A.A.** (2008). Species-specific diversity of a fixed motor pattern: the electric organ discharge of *Gymnotus*. PLoS ONE, 35, e2038. doi:10.1371/journal.pone.0002038.
- Rodríguez-Cattáneo A., and Caputi A. A.** (2009). Waveform diversity of electric organ discharges: the role of electric organ auto-excitability in *Gymnotus* spp. *J. Exp. Biol.* **212**, 3478-3489.
- Sierra F., Macadar O., Buño, W.** (1995) N- type Ca²⁺ channels mediate transmitter release at the electromotor-electrocyte synapses of the weakly electric fish *Gymnotus carapo*. *Brain Research*, **683**, 215 – 220
- Sierra F., Comas V, Buño W., and Macadar, O,** (2005) Sodium-dependent plateau potentials in electrocytes of the electric fish *Gymnotus carapo* *J. Comp. Physiol. A* **191**, 1-11.
- Stoddard, P.** (1999). Predation enhances complexity in the evolution of electric fish signals. *Nature* **400**, 254 -256
- Trujillo-Cenóz, O., Echagüe, J.A. and Macadar, O.** (1984). Innervation pattern and electric organ discharge waveform in *Gymnotus carapo*. *J. Neurobiol.* **15**, 273–281.
- Trujillo-Cenóz, O. and Echagüe, J. A.** (1989). Waveform generation of the electric organ discharge in *Gymnotus carapo*. I. Morphology and innervation of the electric organ. *J. Comp. Physiol. A* **165**, 343–351.
- Westby, G.W.M.** (1974). Assessment of the signal value of certain discharge patterns in the electric fish, *Gymnotus carapo*, by means of playback. *J. Comp. Physiol. A.*, 327-341.
- Watson, D. and Bastian, J.** (1979). Frequency response characteristics of electroreceptors in the weakly electric fish *Gymnotus carapo*. *J. Comp. Physiol. A* **134**, 191 -202
- Yager, D. D. and Hopkins, C. D.** (1993). Directional characteristics of tuberous electrorreceptors in the weakly electric fish *Hypopomus* (Gymnotiformes). *J. Comp. Physiol. A* **143**, 401 -414

Figure Legends

Figure 1. Head to tail EODs waveforms of *Gymnotus*. Waveforms are plotted with head positivity upwards, and normalized and aligned to the peak amplitude of (V_3/P_1). Wave components are labeled using the nomenclatures introduced by Trujillo-Cenóz et al. (1984) and modified by Rodríguez-Cattáneo et al (2008). This scheme is based on the ordinal number of wave components (labeled as V) in the sequence of deflections observed at the head to tail recordings but also by their different origin and mechanisms of generation. Crampton and Albert's (2006) nomenclature (labeled as P_{-1} through P_3) only takes into account the ordinal number of each relative maximum in the head to tail EOD, assigning the position 1 to the main positive peak, thus only the last of the subsequent components of the same polarity are described. The equivalence is $P_{-1}=V_{1ct}$, $P_0 = V_1 + V_2$, $P_1 = V_3$, $P_2 = V_4$, $P_3=V_5$; scale bar = 1 ms. Note that head to tail recordings in water are significantly different from traces obtained with the simple air gap (compare the trace A in this figure with traces A and B of the following figures). This is because although in both cases the head to tail EOD is the weighted sum of the regional electromotive forces, the weighting vector is different in each case. While in the air gap condition is the weighting factor is one for every region, in water it is a function of the ratio between internal resistance of the fish's body region and water resistance (the rationale behind these arguments can be found in Caputi and Budelli, 1995).

Figure 2. *Gymnotus* sp. "carapo PE". A) Head to tail electromotive force (EMF) as recorded in single air gap. One can observe several components before the main positive peak V_3 . This trace is the sum of the EMFs from different body regions. B) Larger magnification of the trace in A illustrates how earlier components V_{1r} , V_{1ct} and V_2 , partially overlap in time. Because of their opposite polarity and different spatial origin, their amplitudes are relatively reduced. C) EMF pattern recorded using the multiple air gap technique shows regional variations in the EOD electromotive force pattern. Note that: i) the weak early components shown in B have different spatial origins; ii) the smooth negative component V_1 occurs mainly in gap 1 but is not seen in the caudal gaps; iii) the weak positive component V_{1ct} , is generated in gaps 4, 5, and 6 (arrows); and iv) the spatial domain of V_2 extends from gap 2 to gap 6. A vertical dotted line was drawn in order to show the progress of the activation along the EO. the Panels D to F show the amplitude of the three main components V_1 - V_2 , V_3 and V_4 as a function of the generator position. The abscissa (x in the fitting expressions) represents the distance between the snout and the middle point between two successive electrodes (expressed as a percentage of fish length). The ordinate represents the peak voltage divided by the inter-electrode percent of total fish length. In this species the EMF of the three components were well fitted by an exponential function: $V_2 = 1.39+1.16*\exp(2.01*x)$,

774 $r^2=0.78$, $V_3 = 0.97+0.05*\exp(7.25*x)$, $r^2=0.75$, $V_4 = 0.11 + 0.03*\exp(8.03*x)$, $r^2=0.88$; $N=27$.
 775 Panels G and H show images obtained from parasagittal sections of silver impregnated EOs (a
 776 collage was made to maintain in focus the relevant features of the electrocytes and their
 777 innervation). At the central region of the fish (gap 4, panel G) *G. sp. "carapo PE"* shows double
 778 innervated electrocytes in the most dorsal column of the EO. The other three rows show simple,
 779 caudally innervated electrocytes of smaller size (concave shape is due to tissue retraction in this
 780 sample). At the tail region all electrocytes are singly innervated (panel H).

781 **Figure 3. *Gymnotus curupira*.** A) Spatiotemporal pattern of electromotive force (EMF) as
 782 depicted by the multiple air gap technique. The EOD of this species has four components (V_1 - V_4).
 783 There is a single early smooth negative component V_1 originated in gaps 1 and 2 (abdominal
 784 region). A vertical dotted line was drawn in order to show the progress of the activation along the
 785 EO. The EMF of the regional peaks is plotted as a function of the position of the generator (in B for
 786 V_1 - V_2 , in C for V_3 , and in D for V_4) as in Fig 2. The spatial contributions to the main peaks were
 787 well fitted by an exponential function: $V_2=0.89+0.75*\exp(2.36*x)$, $r^2=0.83$; $V_3=0.18 +$
 788 $0.35*\exp(4.82*x)$, $r^2=0.85$; $V_4=0.63 + 0.11*\exp(5.83*x)$, $r^2=0.76$; $N=34$. E) Cajal's silver
 789 impregnated material of the central region showing doubly innervated electrocytes at the most
 790 dorsal row and single caudally innervated electrocytes in the three ventral rows (a collage was made
 791 to maintain in focus the relevant features of the electrocytes and their innervation).

792 **Figure 4. *Gymnotus javari*** A) Spatiotemporal pattern of electromotive force (EMF)
 793 recorded using the air gap technique. The rostral EO start with a smooth negative long-
 794 lasting component, barely seen in the htEOD (see Fig 1C). A vertical dotted line was drawn
 795 in order to show the progress of the activation along the EO. B) Detail Multiple of the head
 796 and abdominal waveforms with multiple air gap method show the very rostral origin of V_1
 797 and the abdominal origin of V_3 . In some specimens, including the one illustrated here, the
 798 EOD was followed by some non-constant wavelets (arrow). C, D and E) The EMF of the
 799 regional peaks is plotted as a function of the position of the generator (in C for V_1 - V_2 , in D
 800 for V_3 , and in E for V_4) as in Fig 2 and 3. The early V_1 - V_2 (C) negative wave component
 801 has a bimodal distribution, as indicated by an "eye-fitted" curve. The EMF for V_3 (D) and
 802 V_4 (E) was well fitted by an exponential function: $V_3=0.09+0.27*\exp(4.89*x)$, $r^2=0.80$;
 803 $V_4= 0.35+0.13*\exp(5.99*x)$, $r^2=0.85$; $N=56$.

804 **Figure 5. *Gymnotus javari*. Anatomy of the EO.** A) Superimposed outlines of the
 805 EO as observed in serial horizontal sections of the mouth floor and abdominal wall sections
 806 showing the presence of a rostral expansion of the EO following the caudal limit of the

head as demarked by the cleithrum-opercular aponeurotic sheath. B) Slices taken from another individual in oblique direction (indicated by the red dotted line in A) shows three electrocytes (labeled as 'e') below the cleithrum bone (CB = cleithrum bone, Ao= aorta). C) Parasagittal sections of Cajal's silver impregnated material taken from the middle region of the fish body (gap 4) shows double innervation on caudal and rostral faces of the electrocytes of the dorsal row, and single caudal innervations of the electrocytes at the other three rows. D) Parasagittal section of Cajal's silver impregnations shows two of the four rows (the other two rows were not contained in this section) of caudally innervated electrocytes at the tail region (gap 6). Note a thick posterior electromotor nerve (PEN), wider than the electrocytes (a collage was made to maintain in focus the relevant features of the electrocytes and their innervation).

Figure 6. Detailed analysis of the EOD of *Gymnotus javari*. A) Transcutaneous current pattern showing sinks (blue) and sources (red). Each vertical line (t1 – t6) indicates the time at which the current profiles in panels B to G were measured. The head-to-tail EOD (htEOD) is shown as a reference at the top of A). B) A slow activity caused by a very localized sink at the head region (note that the reversal point, rostral sink – caudal source at t1=1.0 ms before V3 in the htEOD, is located at the head region). C) After a relatively long period of time (t2=0.3 ms before V3), there is an abdominal sink surrounded by two sources, one at the head, and the other distributed along the rest of the body. D) At t3= 0.15 ms before V3, the rostral source is still present, having a distributed sink on the rest of the body. This corresponds to V3r, which is probably generated by the expanded portion of the EO. E) At the peak time (t4=0.0 ms), all the fish's body becomes an extended generator with the reversal point slightly caudal to the center of the fish. F) At t5=0.15 ms after V3 the pattern reverses, as a mirror image of V3 (this corresponds to V4). G) The reversal point of V4 shifts caudally with time (t6=0.35 ms after V3) and a small V5 starts to appear in the head (magnified in the inset). The EOD ends with a small rebound wave at the tail region (caudal V5, pattern not shown).

Figure 7. *Gymnotus obscurus*. This species lacks negative early components preceding the positive peak. A and B) The simple airgap technique shows that while the positive peak (V₃, plot A) is not affected by external load, the negative one (homologous to V₄, plot B) is relatively reduced for large values of the loading resistor. Taking into account our previous experiments on *G. omarorum* (Rodríguez-Cattáneo and Caputi, 2009), we studied this load dependence using a

differential load procedure that allowed us to clamp the external current flow during V_3 (I_3). C) Voltage versus current plots obtained using different clamped I_3 currents show a similar slope (internal resistance) but an electromotive force largely dependent on the clamped current (ordinate value). D) Relationship between the electromotive force of V_4 and the clamped external current during V_3 (I_3). Note that the electromotive force increases more than a 50%. E) The electromotive force pattern shows an exponential growth of V_3 as a function of the generator position (distance from the snout expressed as a percentage of total length, ($V_3 = -6.92 + 5.46 * \exp(3.05 * x)$, $r^2 = 0.93$ $N=7$), and the presence of the small V_4 at the tail region. A vertical dotted line was drawn in order to show the progress of the activation along the EO. F) A single sample obtained from the middle part of the fish (gap 4) was impregnated using Cajal's technique. Sections from this sample show electrocytes innervated only on their caudal faces.

Figure 8. *Gymnotus sylvius* A) Head to tail electromotive force (EMF) as recorded in the single air gap. This trace is the sum of the EMFs from different body regions. Two different components previous to the main positive peak (V_3) can be distinguished: an early negative positive component (V_{1r} , inset red filled regions) followed by a positive one (V_{1ct} , inset blue filled regions). B) Spatiotemporal pattern of electromotive force (EMF) as depicted by the multiple air gap technique. A vertical dotted line was drawn in order to show the progress of the activation along the EO. The EOD of this species has six components (V_{1r} - V_5). There is a single, early, smooth negative component (V_{1r}) originated in gaps 1 and 2 (abdominal region). The positive early component (V_{1ct}) is generated at the transition between the central and tail regions of the fish body (gap 6). C-E) The EMF of the regional peaks is plotted as a function of the position of the generator (in C for V_1 - V_2 , in D for V_3 , and in E for V_4) as in Fig 2, 3 and 5. The spatial contributions to the main peaks were well fitted by an exponential function: $V_3 = 4.22 + 2.67 * \exp(0.81 * x)$, $r^2 = 0.85$; $V_4 = 2.49 + 6.15 * \exp(6.5 * x)$, $r^2 = 0.9$; $N=49$. F) Cajal's silver impregnated material of the central region showing double innervated electrocytes at the most dorsal row (asterisk, see also panel H) and caudally innervated electrocytes in the three ventral rows. G) Caudally innervated electrocytes of the caudal region. As in previous figures a collage was made to maintain in focus the relevant features of the electrocytes and their innervation.. PEN: Peripheral electromotor nerve.

Figure 9. *Gymnotus tigre* A) Spatiotemporal pattern of electromotive force (EMF) recorded by air gap technique in two specimens. Five wave components can be observed (V_1 - V_5). The electromotive force grows exponentially ($V_3 = 0.03 + 3.16 * \exp(3.85 * x)$, $r^2 = 0.96$, $V_4 = -2.23 + 1.41 * \exp(4.78 * x)$, $r^2 = 0.94$; $N=13$). A vertical dotted line was drawn in order to show the progress

of the activation along the EO. B) Parasagittal sections of Cajal's silver impregnated material taken from the middle region of the fish's body (gap 4) show double innervations on the caudal and rostral faces of the electrocytes of the dorsal row, and single caudal innervations of the electrocytes in the other three rows. C) The electrocytes of the tail are innervated only on their caudal faces.

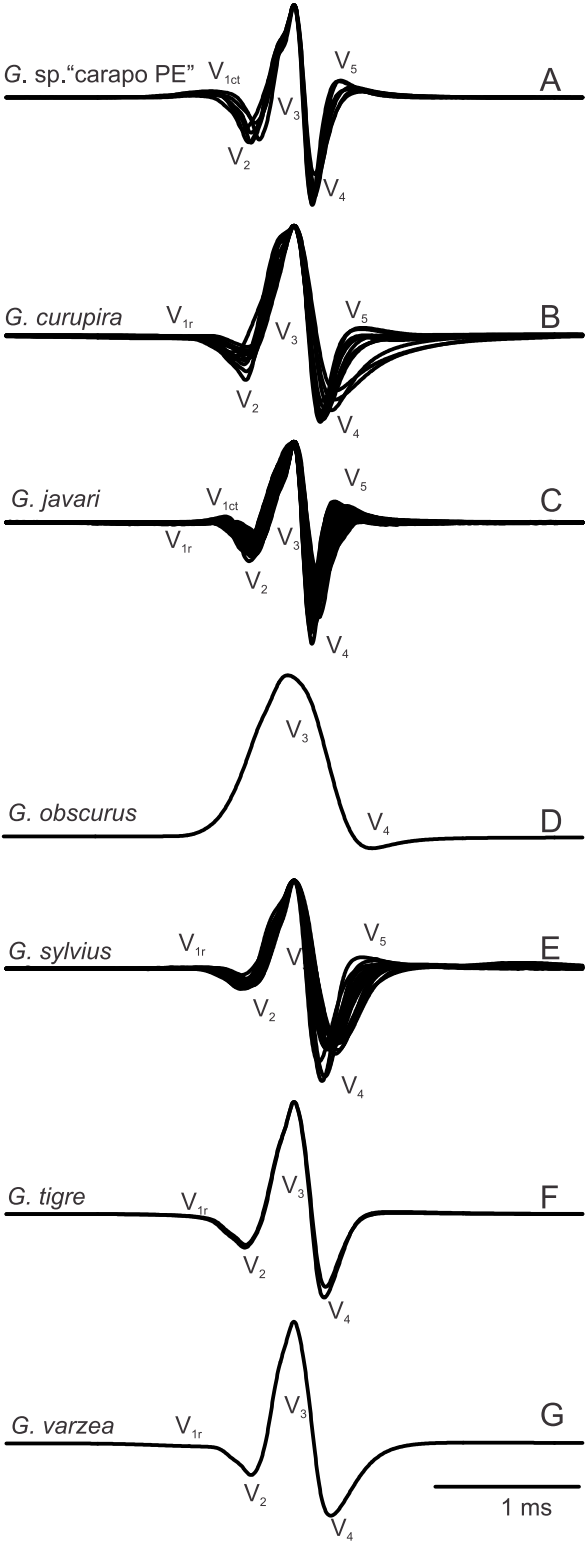
Figure 10. *Gymnotus varzea*. A) Electromotive force pattern registered by air gap technique in one specimen. Four wave components can be observed (V_1 - V_4). In this fish the last (posterior-most) gap was not recorded. A vertical dotted line was drawn in order to show the progress of the activation along the EO. Note the activity of the posterior electromotor nerve at the sixth trace. B) Parasagittal sections of Cajal's silver impregnated material taken from the middle region of the fish's body (gap 4) show double innervations on the caudal and rostral faces of the electrocytes of the two dorsal rows, and single caudal innervations of the electrocytes in the other two rows.

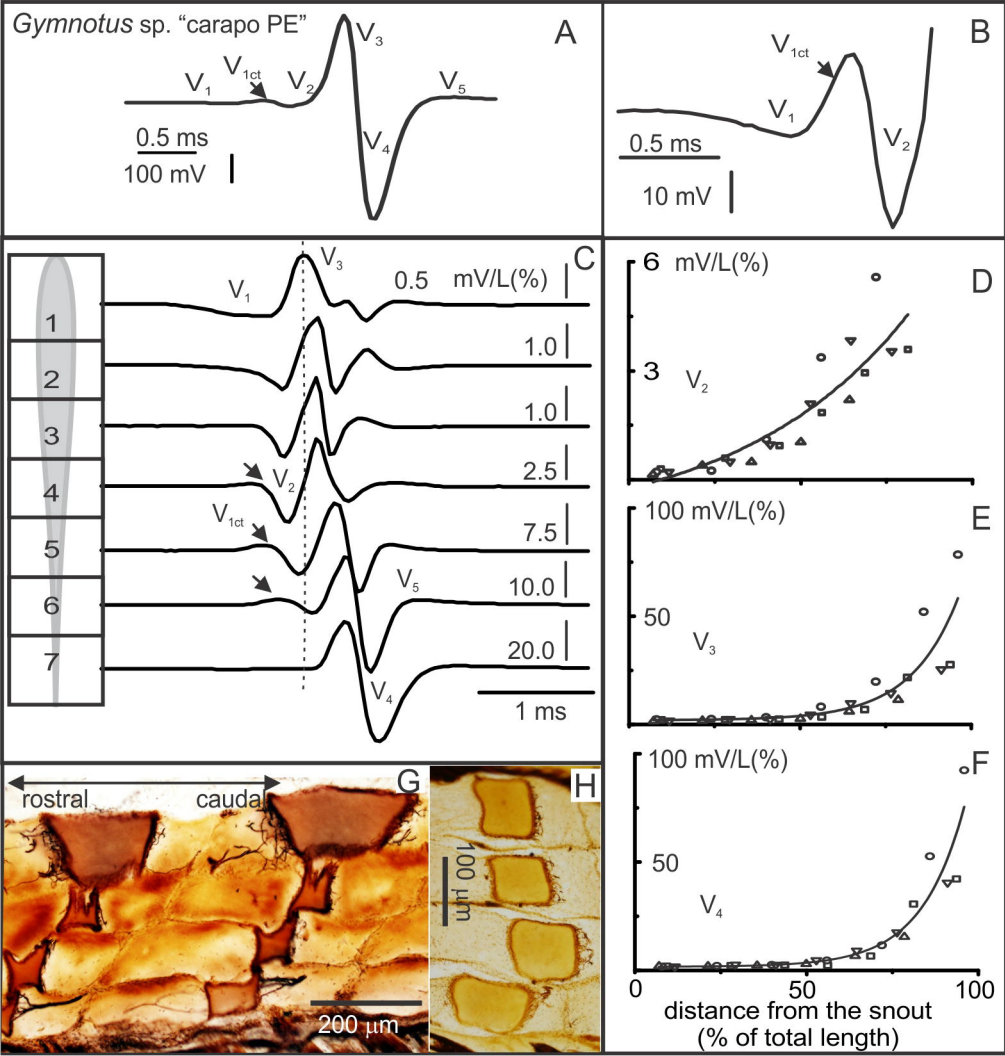
Figure 11. Co-evolution of neural and myogenic mechanisms of wave coordination in *Gymnotus*. The mean of the delay between V_2 and V_3 (t_3-t_2) were plotted against the mean of the delay between V_3 -and V_4 (t_4-t_3), for different species. Symbols indicate the species, bars = standard deviations. Data were obtained from the center region of the fish's body in all cases (gap 4 in this study). The place of capture, numbers of specimens and the range of temperature of the recordings included here are: *G. carapo* SU (Suriname, Rodríguez-Cattáneo et al., 2008): N= 4, T=20-25 °C, *G. sp. "carapo PE"* (Peru) ; N= 4, T= 25-30°C, *G. coropinae* (Suriname, Rodríguez-Cattáneo et al., 2008); N= 10, T= 20-25°, *G. curupira* (Peru): N=8, T=25-30 °C, *G. n. sp. "itu"* (Argentina, Paraná river Rodríguez-Cattáneo and Caputi, 2009); N =12, T=20-25 °C, *G. javari* (Peru) N= 7, T=25-30°C; *G. sylvius* (Argentina, Paraná river, Rodríguez-Cattáneo and Caputi, unpublished) N= 8, T=20-25 °C; *G. omarorum* (Uruguay, Laguna del Cisne Rodríguez-Cattáneo and Caputi, unpublished, summer season) N = 10, T=25-30 °C; *G. omarorum* (Uruguay, Laguna del Cisne Caputi et al., 1993, winter season) N = 8, T=20-25 °C; *G. tigre* (Peru) N=2, 25-30 °C, *G. varzea* (Peru) N= 1, T=25-30 °C.

Table 1. Amplitudes of the head to tail EOD of seven species of *Gymnotus* and the individual wave components V_2 through V_5 Peak to peak amplitude was calibrated in mVcm⁻¹ @10 cm, according to the method described by Franchina and Stoddard (1988). Relative amplitude of the main peaks are normalized by the peak to peak amplitude. EOD's.. Values represent means \pm standard deviations. Asterisk: only 6 out of 9 animals showed V_5 .

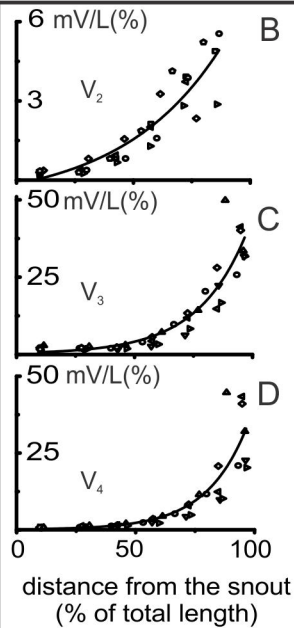
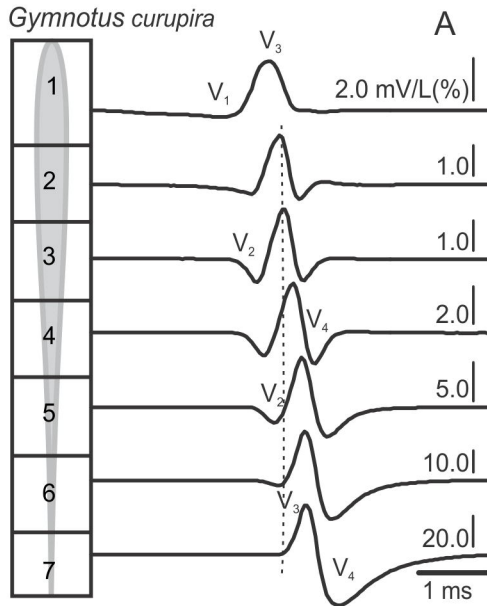
907
908
909
910

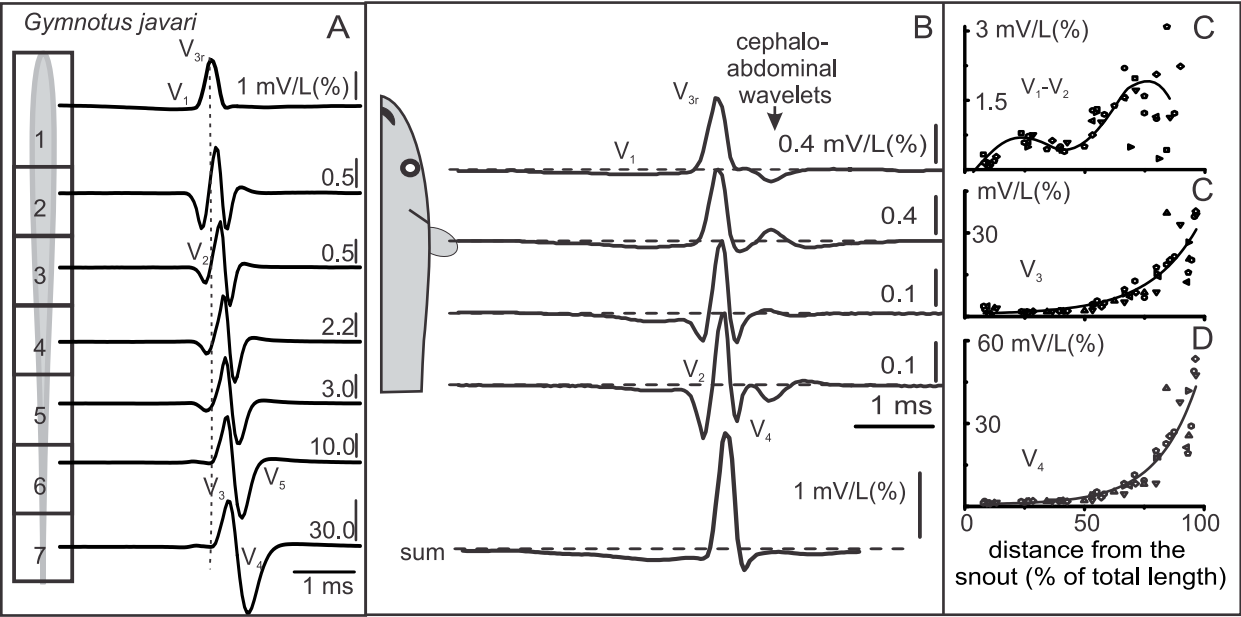
Table 2. The role of five anatomo-functional factors in determining interspecific signal diversity in *Gymnotus*.

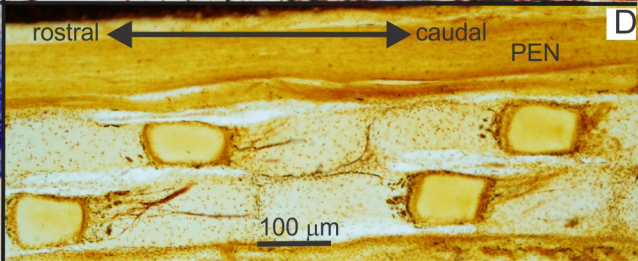
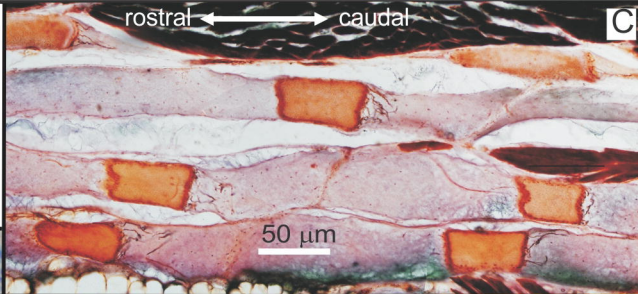
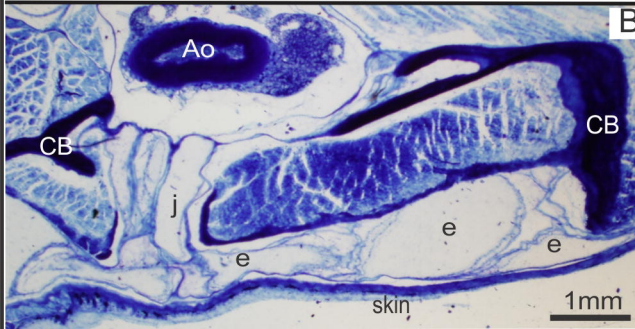
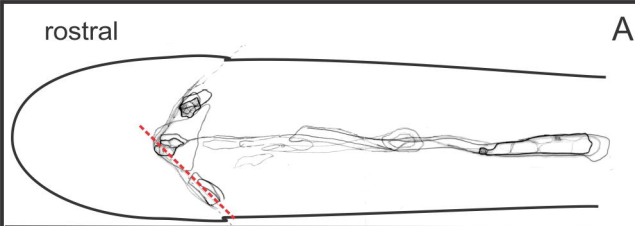


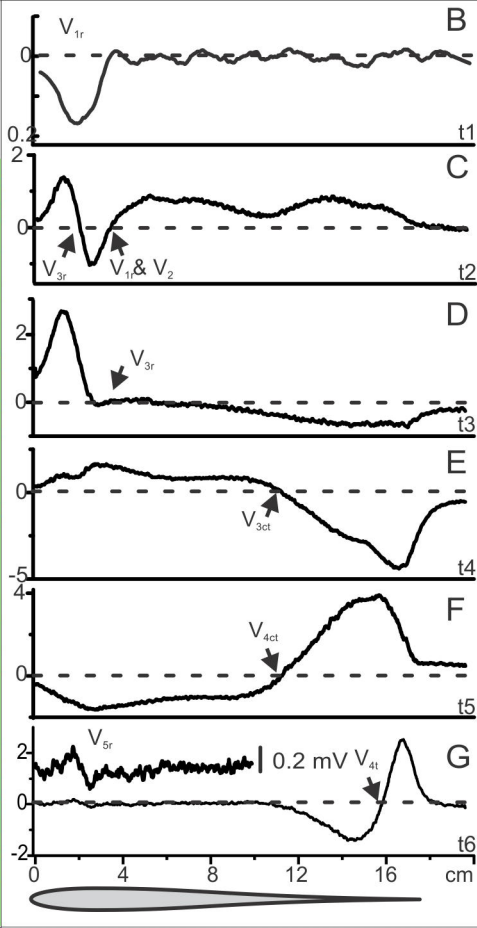
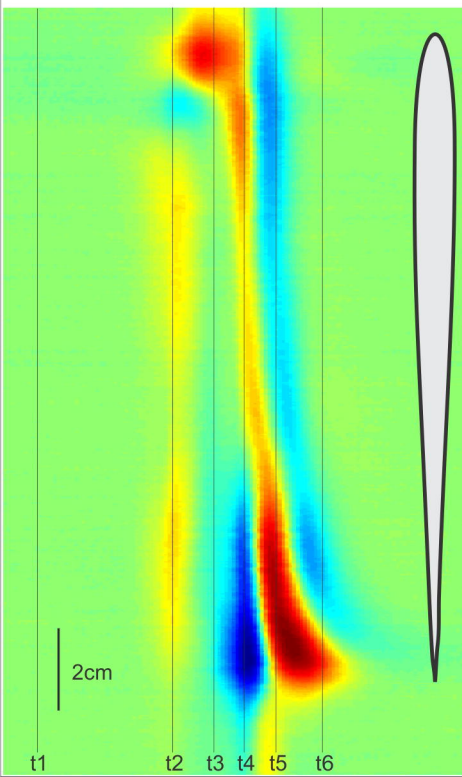


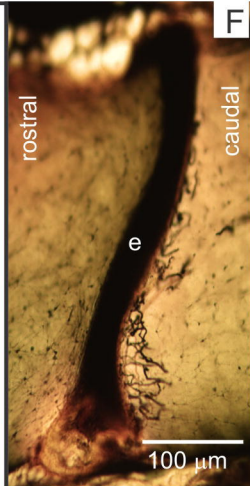
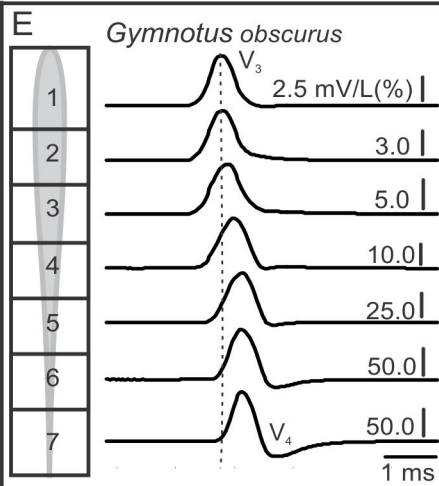
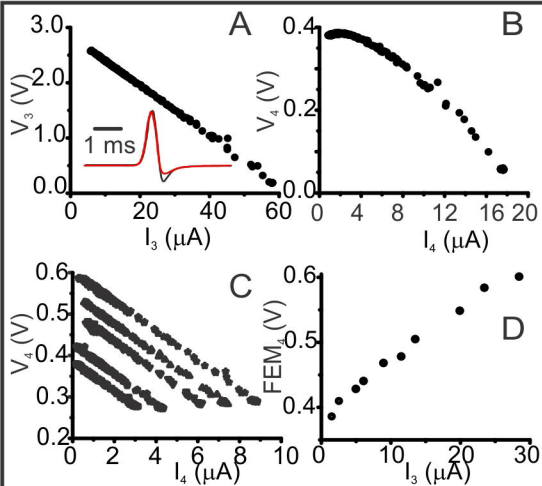
Gymnotus curupira





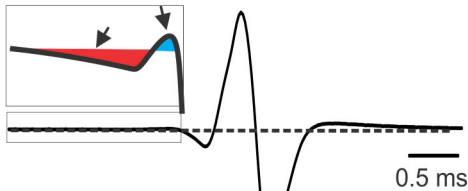




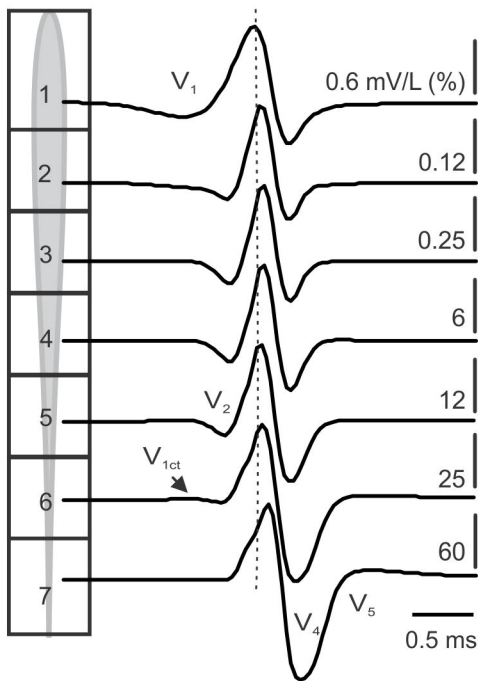


Gymnotus sylvius

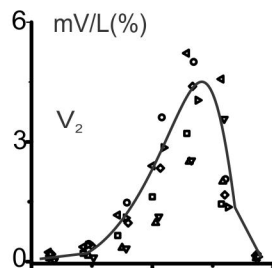
A



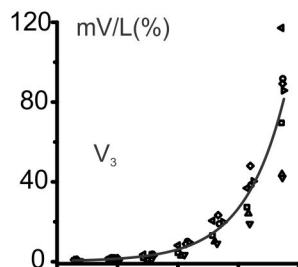
B



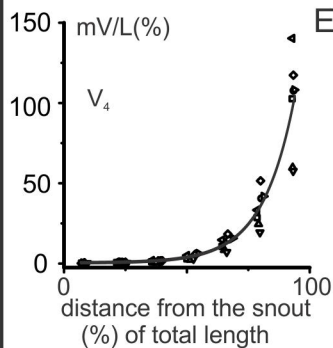
C



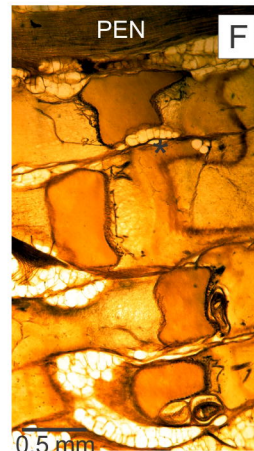
D



E



F

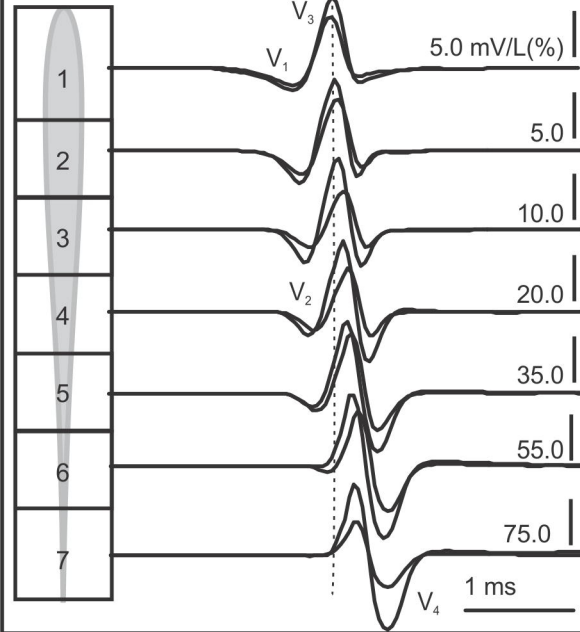


G

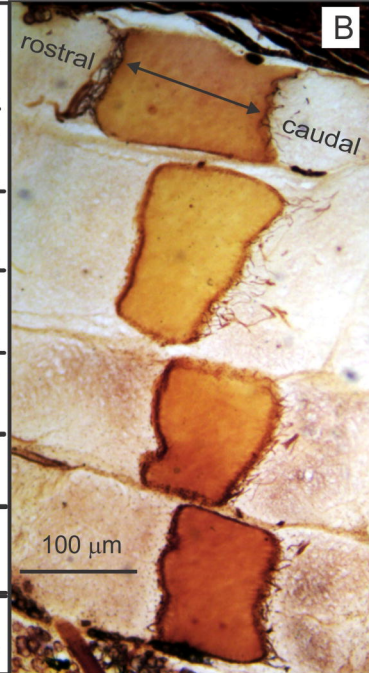


Gymnotus tigre

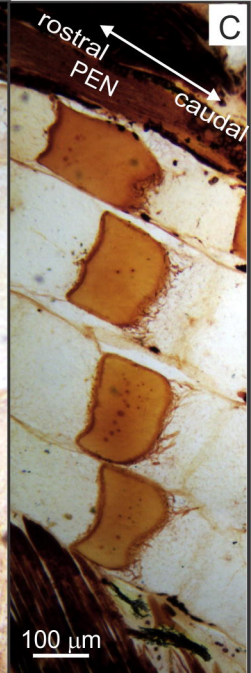
A



B



C



Gymnotus varzea

A

1

V_1

2.5 mV/L (%)

2

2.5

3

V_2

4

4

12

5

20

6

40

7



V_4

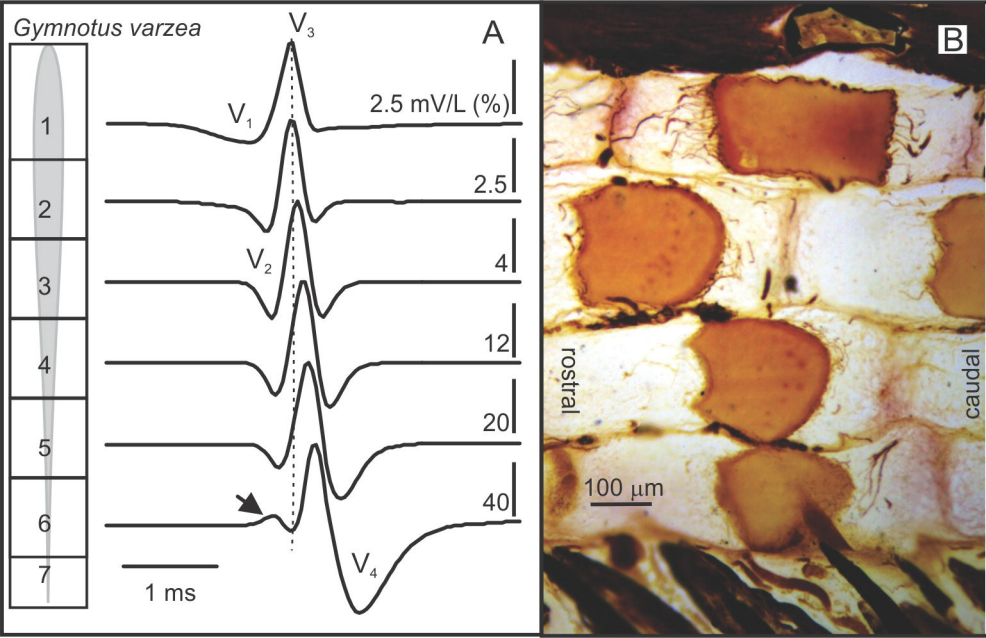
1 ms

B

rostral

caudal

100 μ m



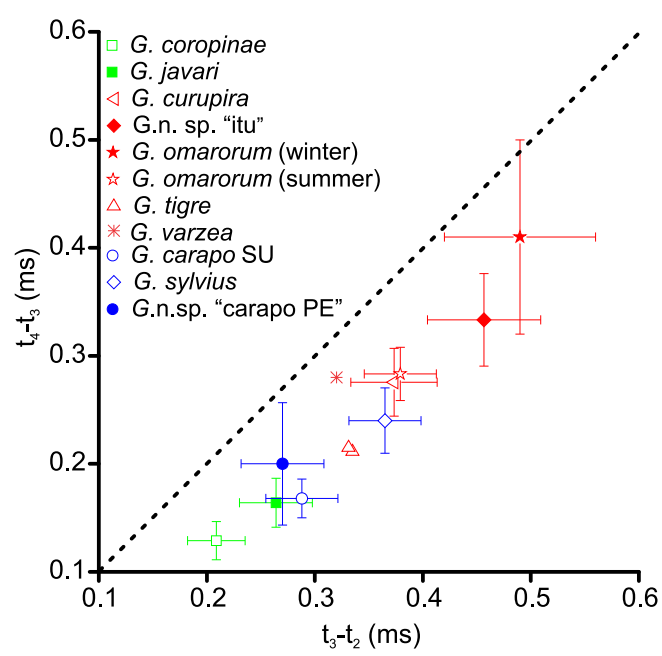


TABLE 1

Species	N	V ₂	V ₃	V ₄	V ₅	PPF (kHz)	Peak to peak (mVcm ⁻¹ @10cm)
<i>G. sp.</i> "carapo PE"	6	-0.203 ± 0.040	0.492 ± 0.030	-0.508 ± 0.030	0.053 ± 0.023	1.990 ± 0.173	135.02 ± 85.27
<i>G. curupira</i>	9	-0.147 ± 0.063	0.602 ± 0.035	-0.398 ± 0.035	0.008 ± 0.014*	1.380 ± 0.107	64.27 ± 25.73
<i>G. javari</i>	119	-0.140 ± 0.031	0.496 ± 0.036	-0.504 ± 0.035	0.061 ± 0.022	1.989 ± 0.173	29.45 ± 13.59
<i>G. obscurus</i>	1		0.939	-0.057			245.03
<i>G. sylvius</i>	17	-0.098 ± 0.022	0.515 ± 0.034	-0.487 ± 0.034	0.006 ± 0.014	1.297 ± 0.173	656.19 ± 258.50
<i>G. tigre</i>	2	-0.169 ± 0.016	0.588 ± 0.024	-0.413 ± 0.025		1.385 ± 0.022	832.66 ± 60.50
<i>G. varzea</i>	1	-0.168	0.628	-0.373		1.218	372.28

TABLE 2.

Functional group	Species	Cellular level			Organismal level	
		Innervation pattern of the electrocyte	Autoexcitability	Neurally generated components	Distribution of electrocyte types	Electrocyte density
I	<i>G. coropinae</i>	Double innervated electrocytes generating V ₂ -V ₃ pattern	High	Not visible at the head to tail EOD	4 clearly distinct regions of EO (in particular one is extended to the head below the cleithrum)	Low
	<i>G. javari</i>					
II	<i>G. curupira</i>	Double innervated electrocytes generating V ₁ -V ₃ pattern at the abdominal region and V ₂ -V ₃ pattern at the central region	Intermediate	Not visible at the head to tail EOD	3 clearly distinct regions of EO.	High
	<i>G. sp. "itu"</i>		High			
	<i>G. omarorum</i>		Low			
	<i>G. tigre</i>		High			
	<i>G. varzea</i>		Intermediate			
III	<i>G. sp. "carapo PE"</i>	Double innervated electrocytes generating V ₁ -V ₃ pattern at the abdominal region and V ₂ -V ₃ pattern at the central region	High	Visible at the head to tail EOD	3 clearly distinct regions of EO.	High
	<i>G. carapo SU</i>					
	<i>G. sylvius</i>					
IV	<i>G. obscurus</i>	Monoinnervated electrocytes	Very low	Not visible at the head to tail EOD	?	?